Exchange across the sediment-water interface quantified from porewater radon profiles

Peter Cook, Valenti Rodellas, Aladin Andrisoa, Thomas Stieglitz

Exchange across the sediment-water interface quantified from porewater radon profiles

Peter G. Cook[a,b], Valentí Rodellas[c], Aladin Andrisoa[c], Thomas C. Stieglitz[c,d],

[a]National Centre for Groundwater Research and Training (NCGRT), School of the Environment, Flinders University, Adelaide SA 5001, Australia

[b]Aix-Marseille Université, IMéRA, Marseille, F-13000, France

[c]CEREGE, Aix-Marseille Université, CNRS, IRD, Coll France, 13545 Aix-en-Provence, France

[d]Centre for Tropical Water and Aquatic Ecosystem Research, James Cook University, Townsville, Queensland 4811, Australia

Corresponding Author: Peter Cook (peter.cook@flinders.edu.au)

HIGHLIGHTS:

- The radon profile method for estimating porewater exchange is reviewed
- A simple recirculation model is presented to aid in profile interpretation
- Uncertainties in the approach are discussed

ABSTRACT

Water recirculation through permeable sediments induced by wave action, tidal pumping and currents enhances the exchange of solutes and fine particles between sediments and overlying waters, and can be an important hydro-biogeochemical process. In shallow water, most of the recirculation is likely to be driven by the interaction of wave-driven oscillatory flows with bottom topography which can induce pressure fluctuations at the sediment – water interface on very short timescales. Tracer-based methods provide the most reliable means for characterizing this short-timescale exchange. However, the commonly applied approaches only provide a direct measure of the tracer flux. Estimating water fluxes requires characterizing the tracer concentration in discharging porewater; this implies collecting porewater samples at shallow depths (usually a few mm, depending on the hydrodynamic dispersivity), which is very difficult with commonly used techniques. In this study, we simulate observed vertical profiles of radon concentration beneath shallow coastal lagoons using a simple water recirculation model that allows us to estimate water exchange fluxes as a function of depth below the sediment-water interface. Estimated water fluxes at the sediment water interface at our site were 0.18 – 0.25 m/day, with fluxes decreasing exponentially with depth. Uncertainty in dispersivity is the greatest source of error in exchange flux, and results in an uncertainty of approximately a factor-of-five.

KEYWORDS: porewater exchange, recirculated seawater, benthic flux, lake, tracers, radon

1. INTRODUCTION

Water recirculation through permeable sediments enhances the exchange of solutes and fine particles between sediments and overlying waters. In particular, it allows for a continuous supply of oxidants and fine particulate and dissolved matter (e.g. dissolved nutrients, bacteria, viruses, phytoplankton) into sediment porewaters, while enhancing the release of degradation products and organisms into overlying waters (Huettel and Rusch, 2000; Huettel et al., 1996). As a consequence, porewater exchange is considered a major contributor to the biogeochemical cycling of surface sediments and overlying waters, particularly in the coastal zone (Anschutz et al., 2009; Huettel et al., 2014, 1998; Jahnke et al., 2005). Porewater exchange increases in importance in highly-permeable sandy sediments, which cover >40% of coastal and shelf areas worldwide (Riedl et al., 1972), where this advective transport of solutes can exceed fluxes driven by molecular diffusion by several orders of magnitude (Huettel and Webster, 2001). This advective exchange between porewaters and overlying waters is caused by pressure gradients at the sediment-water interface, which might be forced by several mechanisms spanning a range of spatial and temporal scales, including wave and tidal pumping, interaction of bottom currents and seafloor topography, density instabilities or pumping activities of benthic fauna (bio-irrigation, Huettel et al., 2014; Santos et al., 2012). For instance, the passage of waves can produce oscillatory flows that interact with bottom topography (e.g. ripples), producing local increases of pressure that drive fluid exchange across the sediment-water interface. In addition, the passage of wave crests and troughs creates pressure

74 gradients over the seafloor that also enhance porewater exchange (Riedl et al.,
75 1972; Rutgers van der Loeff, 1981; Webster, 2003).

76 Despite the importance of porewater exchange in coastal biogeochemical cycles, it
77 is still not easy to quantify the advective flux of water and solutes in permeable
78 sediments (Boudreau et al., 2001; Rocha, 2008). Common methods to estimate the
79 rate of porewater exchange across the sediment-water interface in permeable
80 sediments include (1) deploying automated seepage meters to monitor the
81 porewater flow into overlying waters (e.g. Jahnke et al., 2000; Cable et al., 2006),
82 (2) constructing mass balances in overlying waters for a tracer supplied by
83 porewater inputs (e.g. Stieglitz et al., 2013; Rodellas et al., 2017), (3) injecting
84 artificial tracers or dye into or above the sediments to trace fluid advection across
85 the sediment-water interface (e.g. Reimers et al., 2004; Precht and Huettel, 2004),
86 and (4) modeling the depth profiles of temperature, electrical conductivity or
87 dissolved species in sediments to evaluate the sediment-water exchange rates (e.g.
88 Cable and Martin, 2008; Savidge et al., 2016). Among these dissolved compounds,
89 short-lived, naturally-occurring radionuclides (e.g. ^{224}Ra and ^{222}Rn) have been
90 widely used, mainly because their half-lives are well suited to the common
91 timescales of these porewater exchange processes (e.g. Colbert and Hammond,
92 2008; Cable and Martin, 2008; Cai et al., 2014). Radium-224 (half-life = 3.6 d) is
93 produced by radioactive decay of ^{228}Th, but partitions to aquifer solids which
94 reduces the sensitivity of dissolved ^{224}Ra activities to porewater exchange fluxes.
95 As a noble gas, radon (^{222}Rn; half-life = 3.8 d) is an excellent tracer of porewater
96 exchange because it is not affected by chemical and biological processes occurring
97 within sediments. In this study, we review the application of radon porewater

profiles in sediments to estimate the porewater exchange across the sediment-water interface driven by pressure fluctuations on short time-scales, such as those produced by wave action. We simulate observed radon profiles using a numerical model of water recirculation that allows us to estimate porewater exchange rates as a function of depth below the sediment-water interface, and to explore sensitivity of estimated fluxes to model parameters. An alternative simpler approach is also presented, where water fluxes are estimated based on changes in the observed radon concentration gradient with depth.

2. THEORY

Radon-222 is a natural environmental tracer that has been used for quantifying groundwater inflows to streams and estuaries (e.g. (Cook et al., 2006; Genereux et al., 1993)) and the ocean (e.g. (Cable et al., 1996)) for almost three decades. Radon is produced in the sediments by the radioactive decay of ^{226}Ra, which is part of the ^{238}U decay chain and it is found in the sediment solids and in porewater. After porewater containing radon discharges to surface water bodies, radon activities in the surface water decrease due to gaseous exchange with the atmosphere and radioactive decay. Radon concentrations in surface water are therefore always much lower than concentrations within porewaters. When surface water infiltrates, its dissolved radon concentration will increase, according to

$$\frac{\partial c}{\partial t} = \gamma - \lambda c \qquad (1)$$

where c is the radon concentration, γ is the production rate of dissolved radon, λ is the radon radioactive decay coefficient (0.1818 d^{-1}), and t is time. After a residence time of a few weeks the concentration will reach secular equilibrium, in which the rate of production is exactly balanced by the rate of radioactive decay. The concentration at secular equilibrium is equal to γ/λ. If the radon production rate within the sediments is constant, then the radon concentration in porewater beneath the seafloor will increase with depth, up to a depth where secular equilibrium is reached. The depletion of radon at shallow depths may therefore be used to derive the exchange between porewater and overlying waters.

2.1. Radon deficit model

The most commonly applied approach to estimate the flux of radon across the sediment-water interface is based on the deficit of porewater radon relative to radon concentrations at secular equilibrium, i.e. the radon concentration that would occur without solute exchange (e.g. Martin et al., 2007; Cable and Martin, 2008). This deficit must be equal to the total net flux of radon into overlying waters. More generally, and assuming 1D flow, the net radon flux at depth z' can be written as:

$$J_{Rn} = \int_{z'}^{\infty} (\gamma - \lambda c)\theta dz \qquad (2)$$

where θ is sediment porosity and c is the radon concentration at each depth z. Integrating from z'=0 to ∞ gives the net radon flux across the sediment-water interface.

Aside from the sediment porosity and the radon concentrations at the different depths, this approach requires knowledge of the production rate in sediments (γ), which can either be calculated from slurry-equilibration experiments (Colbert and Hammond, 2008) or derived from deep porewater radon concentrations, which are assumed to be unaffected by porewater exchange (Cable and Martin, 2008).

2.2. Advection cycling model

Exchange of solutes between rivers and lakes and underlying porewaters has frequently been simulated using mass balance models that represent the porewater zone as a perfectly mixed reservoir of constant depth (Bencala, 1983; Cook et al., 2006; Gooseff et al., 2003; Stieglitz et al., 2013). Multiple reservoirs sometimes have been used, although such reservoirs usually operate in parallel so that each reservoir is directly connected to the surface water (Choi et al., 2000). In most cases, the focus of these studies has been on reproducing exchange fluxes rather than porewater concentrations, although Lamontagne and Cook (2007) used a single reservoir model to relate water fluxes to radon concentrations within porewater of a river hyporheic zone that was assumed to be perfectly mixed.

As the objective of the present study is to interpret vertical radon profiles rather than mean porewater concentrations, we consider a series of vertically-stacked reservoirs rather than a single reservoir. This type of model, sometimes referred to as a compartmental mixing model, has been widely applied in soil water and groundwater transport simulations (Adar et al., 1988; Harrington et al., 1999; Kirk and Campana, 1990), but not previously in the context of porewater exchange.

164 Water and solutes are assumed to be perfectly mixed within each cell, and only
165 advective fluxes between the cells are considered. Thus hydrodynamic dispersion
166 is simulated implicitly through mixing within the cells rather than explicitly
167 included in the governing equations. Compartmental mixing cell models have been
168 shown to produce similar results to advective-dispersive models provided that
169 advection is the dominant transport process and that the size of the mixing cell is
170 appropriately chosen (Xu et al., 2007).

171 The model presented here represents a two-dimensional recirculation cell, in
172 which flow reverses periodically. This type of flow system might be produced by
173 the passage of waves across the water surface, with surface water moving into the
174 sediments beneath the wave peaks (high pressure), and exiting beneath the wave
175 troughs (low pressure). We assume that the vertical scale of the recirculation cell
176 is much greater than the horizontal scale, so that horizontal travel times are
177 negligible (this is discussed further below). The two-dimensional model thus
178 collapses into two one-dimensional profiles that exchange water and solutes. The
179 fully saturated porewater zone is discretized into a number of layers (cells), each
180 of which is assumed to be perfectly mixed. Each cell is assumed to continually
181 exchange water with the cells immediately above and below it (the uppermost cell
182 representing the surface water), and also to exchange water with the cell at the
183 equivalent depth in the adjacent profile (Figure 1). The downward flow in one
184 profile is thus balanced by the upward flow in the second profile, and the change in
185 vertical water flux with depth determines the exchange flux between the two
186 profiles. For each profile, we solve

187 $$\frac{\partial(\theta c)}{\partial t} = -\frac{\partial}{\partial z}(q_v c) + \gamma\theta - \lambda\theta c - S \qquad (3)$$

where q_v is vertical water flux (which is a function of depth), and *S* is a mass flux term that allows for flow between the upwelling and downwelling profiles. q_v is defined so that downward fluxes are positive and upward fluxes are negative. Dispersion is not explicitly simulated, but it is implicitly simulated based on the size of the mixing cells. The relationship between cell size (Δz) and implicit dispersivity (α) is given by (Kirchner, 1998; Shanahan and Harleman, 1984):

$$\alpha = \frac{\Delta z}{2} \quad (4)$$

The water flux decreases with depth in the downwelling profile, so that for the first phase of the recirculation cycle, water moves downward on the left hand side and upwards on the right hand side, as shown in Figure 1. Horizontal flows occur from left to right, and are given by

$$q_h(i) = q_v(i-1) - q_v(i) \quad (5)$$

where $q_h(i)$ is the horizontal water flux at the depth represented by cell *i*, $q_v(i-1)$ is the downward water flux into cell *i* from the overlying cell and $q_v(i)$ is the vertical water flux from cell *i* into the underlying cell. Note that both q_v and q_h are volumetric fluxes per square area of the sediment surface, and so q_h is not a Darcy velocity in the traditional sense. Note also that the term *S* in Equation 3 can be obtained by multiplying $q_h(i)$ by the concentration in cell *i* of the downwelling profile. *S* will therefore be positive for downwelling profiles (-S is negative, representing a mass loss) and negative for upwelling profiles (-S is positive, representing a mass gain).

The solute mass balance equations are:

$$\Delta c^a(i) = \Delta t \left[\frac{q_v^a(i-1)}{\theta}\left(\frac{c^a(i-1)-c^a(i)}{\Delta z}\right) + \gamma - \lambda c^a(i)\right] \quad (6)$$

$$\Delta c^b(i) = \Delta t \left[\frac{-q_v^b(i)}{\theta}\left(\frac{c^b(i+1)-c^b(i)}{\Delta z}\right) + \frac{\left(q_v^b(i)-q_v^b(i-1)\right)}{\theta}\left(\frac{c^a(i)-c^b(i)}{\Delta z}\right) + \gamma - \lambda c^b(i)\right] \quad (7)$$

where c is concentration, Δc is change in concentration, q_v and q_h are the vertical and horizontal water fluxes, Δz is the vertical cell dimension, Δt is the temporal discretization and the superscripts a and b denote the fluxes and concentrations in the downward-flow and upward-flow cells respectively (symmetry of the recirculation cell requires that $q_v^a = -q_v^b$).

After a period of time ($t_r/2$), the flow reverses, and so the directions of all arrows shown in Figure 1 reverse. The calculations are then repeated, with superscripts a and b switched in Equations 6 and 7. This cycle is then repeated. Because the direction of flux changes during the recirculation cycle, the mean upward and downward water flux at each depth across a complete recirculation cycle ($\overline{q_v}$) is calculated by dividing q_v by two (i.e. $q_v = 2\overline{q_v}$).

The upper boundary condition is constant concentration ($c=c_0$). The lower boundary is the concentration of radon in equilibrium with the rate of production ($c=\gamma/\lambda$), although in practice the lower boundary is set to be sufficiently deep so that it does not affect simulation results. The key parameters in the model are the concentration in the overlying surface water (c_0), the sediment characteristics (θ, γ), and the characteristics of the recirculation, which include the time for a completed cycle (t_r), and the velocity profile $q_v(i)$.

It should be noted that as the period of the recirculation (t_r) becomes small, radon concentrations derived from the oscillating flow model are equivalent to those observed in a simple 1D steady state model with flow occurring simultaneously in both directions. This is given by

$$\frac{|q_v(i-1)|}{\theta}\left(\frac{c(i-1)-c(i)}{\Delta z}\right)-\frac{|q_v(i)|}{\theta}\left(\frac{c(i)-c(i+1)}{\Delta z}\right)+\gamma-\lambda c=0 \quad (8)$$

2.3. Dispersion model

For small recirculation times (t_r), the solute profiles in a reversing flow field can also be expressed in terms of an enhanced dispersion coefficient, rather than by directly simulating advection (Qian et al., 2009). The flux of radon at any depth can be expressed

$$J_{Rn}=D_e\theta\frac{\partial c}{\partial z} \quad (9)$$

where J_{Rn} is the radon flux and D_e is the enhanced dispersion coefficient ($m^2\ d^{-1}$). Qian et al. (2009) developed a two-dimensional hydraulic model to examine the effect of wave action on porewater solute profiles, and showed that the value of the enhanced dispersion coefficient decreased exponentially with depth, and could be approximated by

$$D_e(z)=\frac{5\alpha Ka}{L\theta}exp\left[\frac{-6.15z}{L}\right] \quad (10)$$

where K is the sediment hydraulic conductivity, a is the half-wave amplitude and L is the wavelength (m).

3. METHODS

3.1. Radon sampling: study site, sampling and analyses

Porewater profiles for radon analysis were collected at La Palme lagoon, located on the western French Mediterranean coastline. La Palme is a small (5 km^2 surface area), shallow lagoon, with mean and maximum water depths of 0.6 and 1.5 m respectively. It is connected with the Mediterranean Sea through a small opening in the coastal sand spit and it receives continuous fresh groundwater inputs mainly from a regional karst aquifer (Stieglitz et al., 2013). The internal mixing of the lagoon and its exchange with coastal waters is driven primarily by the strong north-westerly winds characteristic of the region (regularly exceeding 10 m/s). Tidal forcing plays a minor role on the hydrodynamic functioning of this lagoon (tidal variations in the Mediterranean Sea are usually less than 0.4 m and exchange between the lagoon and the sea is highly restricted). Most of the lagoon is covered by coarse-grained highly-permeable sediments. A recent study conducted by Stieglitz et al. (2013) revealed that wind-driven horizontal pressure gradients at the sediment-water interface produce the recirculation of large amounts of lagoon water through surface sediments. Indeed, they estimated that the equivalent of the volume of the entire lagoon recirculates through the sediments every 25 days. La Palme is thus an ideal site to evaluate the exchange of porewater across the sediment-water interface by using radon porewater profiles.

Porewater samples for radon analysis were collected at 2 different locations (Pz1 at 42.9741°S, 3.0163°E and Pz2 at 42.9391°S, 3.0248°E) using a drive point

piezometer. At each location, samples were collected at depths of 0.05 (only Pz1), 0.10, 0.15, 0.20, 0.30, 0.50, 0.80 and 1.30 (only Pz2) m below the sediment – water interface. 10-mL porewater samples were collected using a gas-tight syringe coupled to the piezometer tubing (minimizing water-air contact) and transferred to 20-mL vials prefilled with a 10-mL high-efficiency mineral oil scintillation cocktail (Cable and Martin, 2008). Concentrations of radon were analyzed by liquid scintillation counting on a Quantulus 1220 with alpha-beta discrimination counting (background of 0.2-0.4 cpm; efficiency of 1.6-2.2, depending on the quenching factor of the sample). Surface water samples (2 L) were collected using a small submersible pump to minimize the gas loss and analyzed using the radon-in-air monitor RAD7 coupled to an extraction system. Samples were decay-corrected to the time of collection.

3.2. Model

The advective compartmental mixing cell model was programmed into Fortran 95. We used a cell size of $\Delta z = 0.01$ m, which is equivalent to an implicit dispersivity of $\alpha = 0.005$ m. The latter is consistent with a flow length of approximately 0.5 m (Gelhar et al., 1992). (This is the approximate depth of radon depletion apparent in the measured profiles, and hence also the apparent depth of recirculation.) Temporal discretization was 10^{-7} days (0.0086 seconds), but identical results were obtained using smaller values. The model was run for at least 20 days, so that radon concentrations reach dynamic equilibrium and are unaffected by initial

296 conditions. Sediment porosity and radon production rate were both assumed to be
297 constant (i.e., do not vary with depth).

298

299 ## 4. RESULTS

300 The two porewater profiles Pz1 and Pz2 showed radon concentrations increasing
301 rapidly with depth up to around 30 - 50 cm depth. Radon concentrations below
302 these depths were relatively constant, with maximum concentrations of
303 approximately 5000 Bq m^{-3} and 2500 Bq m^{-3} for Pz1 and Pz2 respectively, which
304 likely reflect concentrations reaching secular equilibrium. The lower value
305 observed at 0.8 m for PZ1 is likely due to analytical or sampling uncertainty or may
306 reflect a spatial variation in the radon production rate. The difference between the
307 measured radon concentrations at shallow depth and these equilibrium
308 concentrations sustained by the production rate indicates that there is a significant
309 exchange of radon between porewaters and overlying waters.

310

311 ### 4.1. Deficit model

312 The radon production rates for the two sites are approximately 900 and 450 Bq m^3
313 d^{-1} for Pz1 and Pz2, respectively, as derived from the maximum concentrations
314 measured at each site (assuming constant production rates over depth). By
315 applying equation 2 and using a porosity (θ) of 0.4, we estimated a total net flux of
316 radon into overlying waters of 58 and 38 Bq m^{-2} d^{-1} for Pz1 and Pz2, respectively.

The radon flux estimated here refers to the total net loss of radon from sediments into surface waters and thus includes also the flux of radon supplied by molecular diffusion. The net advective-dispersive flux of radon from sediments can be calculated as the difference between the estimated total flux and the diffusive flux, which can be approximated using Fick's First Law and radon diffusion coefficients corrected for both temperature and tortuosity ($\sim 1 \times 10^{-4}$ m^2 d^{-1}; (Boudreau, 1997; Li and Gregory, 1974)). By using the radon gradients over depth measured in the shallowest porewaters (above 20 cm), the diffusive flux is on the order of 10^{-1} Bq m^{-2} d^{-1}, which is 2 orders of magnitude lower than the total radon flux. Therefore, radon diffusive fluxes in the studied profiles can be neglected and the total ^{222}Rn flux can be attributed to advective-dispersive fluxes.

4.2. Advection cycling model

Observed radon profiles were simulated using constant surface water concentrations of 30 (Pz1) and 90 (Pz2) Bq m^{-3}, and $q_v(z)$ and t_r were varied in a trial-and-error fashion, until good fits with observed profiles were obtained. It was found that best-fits to radon profiles were produced with water fluxes that decreased exponentially with depth, and so this was adopted in all simulations.

The simulated radon profile for Pz1 is shown in Figure 3, and closely matches the observed profile to a depth of 0.5 m. This simulation uses a recirculation time of $t_r/2 = 10^{-5}$ days (0.864 seconds), although identical profiles are produced for recirculation times on the order of $<10^{-2}$ days. For longer times, different upwelling and downwelling profiles are obtained (Figure 4). In this case, the

340 profile that has just completed its downwelling phase (orange line in Figure 4) has
341 much lower concentrations than the upwelling profile (blue line). This essentially
342 represents differences that would be observed depending on the sampling time in
343 relation to the phase of the cycling.

344 The mean upwelling or downwelling water flux across the sediment – water
345 interface in Pz1 is $\overline{q_v}(0)$ = 0.25 m d^{-1} (3×10^{-6} m s^{-1}). The radon flux from the
346 surface into the underlying cell is $\overline{q_v}(0)c(0)$, which is equal to 7.5 Bq m^{-2} d^{-1}. The
347 radon concentration in this second cell (immediately below the surface water
348 layer) is 240 Bq m^{-3}, and so there is also an upward radon flux into the surface
349 water of $\overline{q_v}(0)c(1)$ = 61 Bq m^{-2} d^{-1}. The net radon flux into the surface water is
350 therefore $\overline{q_v}(0)[c(1) - c(0)]$ = 54 Bq m^{-2} d^{-1}. This is essentially the same as the
351 radon flux for Pz1 calculated from Equation 2 (58 Bq m^{-2} d^{-1}).

352 Figure 5 depicts the sensitivity of the radon profiles to variations in surface water–
353 sediment exchange flux ($\overline{q_v}(0)$), attenuation of water flux with depth (k), and
354 implicit dispersivity. The latter is investigated by varying the cell dimensions in the
355 model. The simulations show, that if dispersivity is fixed, then if sampled with
356 sufficient resolution, the radon profiles allow unique determination of $\overline{q_v}(0)$ and k,
357 as these parameters affect the profiles in different ways. In particular, varying k
358 only affects the deeper parts of the profile. However, dispersivity and velocity
359 affect radon profiles similarly, indicating model non-uniqueness. Assuming a value
360 for dispersivity is therefore essential for estimating the water flux. In our case,
361 fitting the radon profiles with dispersivities of 0.0025 and 0.01 m^2 d^{-1} (cell sizes of
362 0.005 and 0.02 m, respectively) would have resulted in mean surface water fluxes
363 of 0.5 and 0.125 m d^{-1} m respectively.

Additionally, the uncertainties associated with radon analytical measurements allow for accommodating different radon profiles (for a fixed dispersivity), and thus yield different simulated k and $\overline{q_v}$ values (Figure 6). Thus, within the error bars of the radon measurements, surface water fluxes of $\overline{q_v}(0)$ = 0.2 – 0.35 m d^{-1} and flux attenuation rates of k = 0.5 – 15 m^{-1} are possible. However, the lowest values of k are only possible if the two shallow radon values (< 0.15 m depth) are towards the upper limit of the analytical uncertainty range, and the four deeper values (0.15 – 0.5 m) are towards the lower limit. The reverse applies for the higher values of k. This is extremely unlikely to be the case (probability of 2^{-6}; or less than 2%). Thus, the true uncertainty in k is much less than this, and probably closer to $2.0 < k < 10$ m^{-1}. Values of k are most sensitive to radon concentrations at 0.2 – 0.4 m depth (Figure 5), and increasing the precision of these measurements would significantly improve the accuracy of the flux attenuation rate estimate.

Radon concentrations in profile Pz2 are reproduced using a production rate of γ = 450 Bq m^{-3} d^{-1}, and surface flux $\overline{q_v}(0)$ = 0.18, but with other parameters identical (θ = 0.4; $t_r/2 = 10^{-5}$ d (0.86 s); with k = 5 m^{-1}).

4.3. Dispersion Model

It is also possible to represent the observed radon data in terms of enhanced dispersion coefficients rather than explicitly considering advective fluxes. By equating Equations 2 and 9, we obtain

$$D_e \theta \left.\frac{\partial c}{\partial z}\right|_{z=z'} = \int_{z'}^{\infty} (\gamma - \lambda c)\, \theta dz \qquad (11)$$

386 The dispersivity profile can therefore be obtained by approximating $\frac{\partial c}{\partial z}$ using the
387 observed changes in radon concentration between sampling depths and solving
388 Equation 11.

389 The profile of enhanced dispersion coefficient calculated for profile Pz1 in this way
390 is depicted in Figure 7a. The dispersion coefficient is related to the flux by
391 $D_e = |v|\alpha$, where ν is the water velocity. As dispersion will occur under both
392 upward and downward flow, it is therefore related to the recirculation flux
393 according to

394 $$D_e = \frac{q_v \alpha}{\theta} = \frac{2\overline{q_v}\alpha}{\theta} \quad (12)$$

395 where q_v is the upward or downward flux that occurs during respective upwelling
396 and downwelling phases, and $\overline{q_v}$ is the mean upward or downward flux averaged
397 across the two phases. Thus we can calculate the average flux $\overline{q_v}$ by rearranging
398 equation 12. This is shown in Figure 7b, where it is also compared with the flux
399 profile obtained from the advection cycling model. The surface flux calculated
400 using Equations 11 and 12 is 0.31 m d^{-1}, which is similar to that calculated from the
401 mixing cell model (0.25 m d^{-1}).

402

5. DISCUSSION

5.1. Model sensitivity

The results from both the advection cycling and the dispersion model are a function of the selected longitudinal dispersivity (expressed as cell size for the advection cycling model). Changing the selected dispersivity will result in proportional changes on the estimated water fluxes. Since dispersivity is a scale dependent parameter, longitudinal dispersivity (α) has been often related to the length of the flow path at the field scale (Gelhar et al., 1992; Neuman, 1990). Assuming a flow path length of 0.5 m, we would obtain an approximate dispersivity of 0.005 m, which is the value used in this study. The estimated dispersivity would largely depend on the length scale selected, which may be difficult to define when dealing with porewater fluxes. As an alternative approximation, Qian et al. (2008) suggested that pore-scale dispersivities in a sediment bed can be approximated by the average particle size. Since the sediment of the study site are mainly composed by coarse-grained particles, the mean particle size is likely ranging from half to a few millimeters, and the expected range of α would therefore be on the order of 0.001 m. This gives a factor-of-five uncertainty in α, and hence also in water flux.

Aside from longitudinal dispersivity, which is the single most important control on model results, the advection cycling model is also sensitive to other input parameters. Although exchange flux ($\overline{q_v}$) is proportional to porosity (θ), this parameter is relatively easy to estimate in unconsolidated sediments, and it is not expected to vary in a wide range. The radon production rate (γ) is constrained by the radon concentrations measured in deep porewaters, and so it is important for

427 samples to be collected from sufficient depth. In our example, γ was assumed to be
428 constant with depth, although variations in θ and γ with depth can be introduced to
429 the model if they are expected to occur. In this case, γ would need to be derived
430 from equilibration experiments, and previous studies have shown that these
431 measurements can have significant uncertainties (Key et al., 1979; Berelson et al.,
432 1982). Model-derived water fluxes in the uppermost layers of the sediment are
433 relatively insensitive to the selected production rate (γ), but γ exerts an important
434 control on the water fluxes simulated for deeper layers, where radon
435 concentrations approach secular equilibrium. Accurate estimation of water fluxes
436 at depth, and the rate (and functional form) of flux attenuation, is also highly
437 sensitive to the analytical precision of radon measurements. We assumed that $\overline{q_v}$
438 decreased exponentially with depth, as this is commonly assumed (e.g. Qian et al.,
439 2009; Fram et al., 2014; Wilson et al., 2016) and because the exponential decrease
440 produced the best fit to the data. Finally, the model is not very sensitive to
441 variations in the time for each phase for the cycle when t_r is on the order of $<10^{-2}$
442 days. For a given value of dispersivity, the uncertainty in all these input
443 parameters and analytical precision result in an uncertainty in the water flux
444 across the sediment – water interface ($\overline{q_v}(0)$) of approximately a factor-of-two.
445 Thus, as previously discussed, uncertainty in dispersivity dominates the
446 uncertainty in surface water flux.

447 A limitation of the model is that it neglects horizontal travel times between
448 downwelling and upwelling profiles. This may be reasonable for small-scale
449 recirculation driven by wave action, as at any time upwelling and downwelling
450 zones are likely to be separated by only a few centimetres. The assumption is less

likely to be valid for recirculation systems driven by processes operating over longer timescales, such as seiches or tides. For these, porewater concentrations (such as those shown in Figure 4) are likely to be underestimated, particularly for upwelling profiles.

5.2. Quantification of water exchange across the sediment-water interface

A number of previous studies have estimated net radon fluxes across the sediment–water interface by integrating the radon deficit in sediment porewater (Equation 2) (e.g. Cable and Martin, 2008; Martin et al., 2007). However, it is not straightforward to calculate the water flow from this data. The common approach to convert this radon flux into specific porewater discharge is by dividing the mass flux by the radon concentration in the shallowest porewater sample (Cable and Martin, 2008; Martin et al., 2007). Given that it is extremely difficult to collect porewater samples for radon analysis in the top centimeters of the sediment, the nearest-surface porewater samples are commonly collected at 0.05-0.1 m depth. In the case of the profiles collected in La Palme lagoon, the radon concentration in the uppermost porewater sample in PZ1, which was collected at a depth of 0.05 m, is 930 Bq m^{-3}. Had we followed this approach to estimate the water exchange between porewater and overlying waters, we would have obtained a flow of 0.06 m d^{-1}, which would underestimate the water flow derived from the advection cycling model ($\overline{q_v}(0)$ = 0.25 m d^{-1}) by a factor of approximately 4 (or by a factor of 8 if the shallowest sample was collected at 0.1 m depth). The main difference

474 between these estimates is that the midpoint of the uppermost cell for the
475 advection cycling model is at a depth of 0.005 m (with a simulated radon
476 concentration of 240 Bq m^{-3}), which is a depth virtually impossible to sample for
477 radon analysis. Although the concentration difference between the uppermost cell
478 and the surface water must be considered to estimate the water exchange rate, the
479 surface water concentrations are often small when compared with porewater
480 concentrations. Thus, whilst the commonly applied radon deficit approach allows
481 estimating net radon fluxes across the sediment-water interface, water fluxes are
482 more accurately quantified by modeling the radon distribution with depth. An
483 alternative approach is to calculate the dispersion coefficient by dividing the net
484 radon flux at each depth by the concentration gradient. Even if samples are
485 collected from below 5 cm, the dispersion coefficient calculated in this way does
486 not appear to greatly underestimate the dispersion coefficient at the sediment –
487 water interface. This is because $\frac{\partial c}{\partial z}$ varies more slowly with depth than does *c*. The
488 water flux can then be estimated by dividing the surface dispersion coefficient by
489 the dispersivity.

490 One of the advantages of the radon approach described here is that it allows the
491 estimation of water fluxes as a function of depth. However, as discussed above, an
492 accurate estimation of exchange fluxes at deeper depths would require more
493 precise radon measurements (e.g. counting deep radon porewater samples for
494 longer times), increased sampling resolution and/or radon equilibration
495 experiments (Colbert and Hammond, 2007) to provide independent estimates of
496 the radon production rate. While most of the porewater exchange studies have
497 focused on the fluxes across the sediment-water interface, determining the

exchange fluxes at deeper depths is important for understanding the biogeochemical cycles in sediments. The penetration depth of reactants (e.g. oxygen), for example, will depend on the advective porewater velocities, as well as on the consumption/production rates in the sediment layers (Precht et al., 2004).

The approaches described in this paper are most appropriate in those systems where the driving force generating horizontal pressure gradients at the sediment-water interface oscillates in relatively short temporal scales (seconds to hours). Larger recirculation times (hours to days) would result in profiles that would significantly change depending on the sampling time in relation to the phase of the advection cycle (upwelling or downwelling) (Figure 4). The proposed approaches are thus best suited to quantifying porewater exchange fluxes produced by the undulating pressure at the seafloor generated by gravity waves interacting with relatively flat sediment surfaces. These models implicitly include the effects of interaction between wave-driven oscillatory flows and seabed morphology, which may significantly enhance water recirculation through sediments, particularly in areas with a water depth shallower than half the wavelength of the wave (Precht and Huettel, 2003). However, if bedforms (e.g. ripples) are stable on timescales of hours or longer, this might give rise to stable zones of up- and downwelling, and so profiles would vary depending on the area of collection. Note that bottom topography can change significantly over short time scales (e.g. ripple migration), particularly during strong periodic events (e.g. storms) or in areas affected by strong bottom currents (Precht et al., 2004; Savidge et al., 2008). Therefore, zones of upwelling and downwelling porewater in permeable sediments would also propagate with ripple migration (Precht et al., 2004). This intensive lateral shifting

of up- and downwelling zones within the sediment together with horizontal diffusion and dispersivity may contribute to homogenizing the vertical profiles. In a similar manner, areas of preferential resuspension or deposition of sediments could also release or trap significant volumes of porewaters (Santos et al., 2012), and thus would also result in significantly different porewater profiles depending on the sampling area. Collecting different radon porewater profiles in the same area should provide additional information on the temporal and spatial scales of the driving forces, by identifying the stability of upwelling and downwelling zones.

The advection cycling and the dispersion models represent thus a reliable method to characterize water exchange across the sediment-water interface driven by pressure gradients reversing at short temporal scales. Radon has advantages over other porewater tracer approaches, as it is more sensitive to low exchange fluxes than temperature (Briggs et al., 2014), and is simpler than dye injection approaches. Other methods commonly applied to quantify porewater exchange are not well suited to the estimation of fluxes with such short residence times. In situ seepage meters may alter fluxes above and below the sediment interface due to the presence of the instrument. This might not be significant for fluxes driven by longer-scale pressure changes, but is likely to be important for processes operating on very short time-scales. Tracer mass balances in overlying waters require estimation of the concentration of exchanging water to convert the tracer mass balance to a water mass balance. The appropriate end-member concentration will depend on the hydrodynamic dispersivity for this method, as it does for porewater tracer methods. However, mass balances in overlying waters will have additional uncertainties due to the need to also define other components of the mass balance.

546

547 5.3. Model-derived results for La Palme Lagoon

548 The shape of the radon porewater profiles collected in La Palme Lagoon (Figure 2)
549 suggests that porewater exchange at the sites sampled is driven by pressure
550 gradients reversing at short temporal scales (up to hours). Larger reversing scales
551 would have produced radon profiles similar to those shown in Figure 4. The
552 enhanced diffusion coefficients at the surface water – sediment interface
553 calculated from the advection cycling model ($D_e = 2\overline{q_v}\alpha\theta^{-1}$ = 0.006 m^2 d^{-1} for Pz1
554 and 0.004 for Pz2) or estimated from Equation 11 (0.008 m^2 d^{-1} for Pz1 and 0.008
555 m^2 d^{-1} for Pz2) can be compared with the relationship derived by Qian et al. (2009)
556 and reproduced in Equation 10. Using the simulated attenuation rate (5 m^{-1}), we
557 obtain 6.15/L = 5 m^{-1}, and hence L ≈ 1.2 m. Similarly,

558 $$\frac{5\alpha K a}{L\theta} \approx 0.004 - 0.008 \text{ m}^2 \text{ d}^{-1} \quad (13)$$

559 Using α = 0.005 m, θ = 0.4, and assuming a = 0.05 m then gives K ≈ 1.5 - 3.1 m d^{-1}.
560 These are typical values of hydraulic conductivity for saturated silty sands (Freeze
561 and Cherry, 1979), such as those found in La Palme Lagoon. Therefore, the
562 observed surface dispersion coefficient and velocity and their rate of attenuation
563 with depth is consistent with wave action being the principle driver for
564 recirculation in La Palme Lagoon. Since wave dynamics in La Palme Lagoon are
565 mainly controlled by the wind regime, wind forcing appears to be an important
566 driver of porewater exchange in this lagoon, as already suggested by Stieglitz et al
567 (2013). Future studies should focus on evaluating the temporal variability of water

568 and solute fluxes across the sediment-water interface in different wind (wave)
569 conditions.

570 Considering that the water depths of La Palme lagoon usually range from 0.3 to 1.5
571 m, the figures estimated in this study would imply that the entire lagoon volume
572 would recirculate through sediments every few days. These recirculation fluxes
573 may therefore have important implications for the functioning of this coastal
574 lagoon, since they may enhance the exchange of oxygen, solutes and particle-
575 associated compounds between sediment and the overlying water column
576 (Anschutz et al., 2009; Huettel and Rusch, 2000; Huettel et al., 1996; Jahnke et al.,
577 2005). Accurately evaluating these recirculation fluxes is therefore required to
578 understand the role that this process may play on the biogeochemical cycles of
579 lagoon water and sediments.

580

581 ### 5.4. Extension to Other Radionuclide Tracers

582 Within the last few years, a number of studies have used the $^{224}Ra/^{228}Th$ ratio in
583 coastal sediments to calculate the ^{224}Ra flux and the corresponding water flux
584 across the sediment-water interface (Cai et al., 2012, 2014, 2015). Unlike ^{222}Rn,
585 ^{224}Ra and ^{228}Th will partition onto the solid phase, and so the ^{224}Ra deficit must be
586 calculated from the total exchangeable ^{224}Ra and ^{228}Th activities, rather than from
587 ^{224}Ra and ^{228}Th dissolved in pore water. However, calculation of water fluxes from
588 ^{224}Ra and ^{228}Th profiles also requires information on ^{224}Ra activities in the
589 dissolved phases, as only this component will be transported with the water. In
590 addition, the partitioning of ^{224}Ra between water and solid phases is largely

591 dependent on the chemical composition of porewaters (e.g. salinity, pH,
592 temperature, redox potential) and the characteristics of the sediments (e.g. grain
593 size, fraction of exchangeable sites, content of iron and manganese), requiring an
594 appropriate characterization of the ^{224}Ra solid-solution partitioning coefficients
595 (Beck and Cochran, 2013; Gonnea et al., 2008). Finally, it should be noted that
596 partitioning to the solid phase means that depletion of ^{224}Ra in pore water will be
597 much shallower than for ^{222}Rn (as depleted ^{224}Ra in pore water will be replaced by
598 ^{224}Ra released from the sorbed phase), and so this requires much finer resolution
599 sampling.

600 Recent studies using the $^{224}Ra/^{228}Th$ method have been mainly in finer grained
601 sediments than those that have used the ^{222}Rn method, and in these environments
602 diffusion often forms a significant component of the tracer flux. The advection
603 cycling model presented in this paper is less amenable to situations in which
604 molecular diffusion is a significant component of the tracer flux. However,
605 notwithstanding the above limitations, in advection-dominated systems, numerical
606 models similar to that presented in this paper could potentially be used to estimate
607 the variation in water flux with depth based on measured ^{224}Ra profiles.

608

609 ## 6. CONCLUSIONS

610 We simulated radon porewater profiles using an advective cycling numerical
611 model to improve estimates of the flux of radon and water between sediments and
612 overlying waters. This model is based on a series of radon mass balances in
613 vertically-stacked reservoirs and where radon profiles are governed by advective

614 porewater fluxes that reverse periodically. The model allows estimation of water
615 fluxes at different depths, which may provide some insights on the overall
616 penetration depth of recirculation processes and the biogeochemical cycling in
617 sediments. A simpler approach, based on the estimation of dispersion coefficients
618 from the radon concentration gradient with depth, can also provide reasonable
619 estimates of the advective water flux.

620 The proposed approaches are well suited to evaluate porewater fluxes driven by
621 pressure gradients reversing at short temporal scales (up to hours), such as those
622 produced by waves and semidiurnal tides, and in areas with no permanent
623 bedforms that create preferential flow cells. Other methods commonly applied to
624 quantify benthic fluxes (e.g. tracer mass balance in overlying waters, seepage
625 meters) are not well suited to the estimation of fluxes with such short time-scales.

626

627

7. REFERENCES

Adar, E.M., Neuman, S.P., Woolhiser, D.A., 1988. Estimation of spatial recharge distribution using environmental isotopes and hydrochemical data, I. Mathematical model and application to synthetic data. J. Hydrol. 97, 251–277. doi:10.1016/0022-1694(88)90119-9

Anschutz, P., Smith, T., Mouret, A., Deborde, J., Bujan, S., Poirier, D., Lecroart, P., 2009. Tidal sands as biogeochemical reactors. Estuar. Coast. Shelf Sci. 84, 84–90. doi:10.1016/j.ecss.2009.06.015

Beck, A.J., Cochran, M.A., 2013. Controls on solid-solution partitioning of radium in saturated marine sands. Mar. Chem. 156, 38–48. doi:10.1016/j.marchem.2013.01.008

Bencala, K.E., 1983. Simulation of solute transport in a mountain pool-and-riffle stream with a kinetic mass transfer model for sorption. Water Resour. Res. 19, 732–738. doi:10.1029/WR019i003p00732

Berelson, W.M., Hammond, D.E., Fuller, C., 1982. Radon-222 as a tracer for mixing in the water column and benthic exchange in the southern California borderland. Earth Planet. Sci. lett., 61, 41-54.

Boudreau, B., 1997. Diagenetic models and their implementation: modelling transport and reactions in aquatic sediments. Springer, Berlin, Heidelberg.

Boudreau, B.P., Huettel, M., Forster, S., Jahnke, R.A., McLachlan, A., Middelburg, J.J., Nielsen, P., Sansone, F., Taghon, G., Van Raaphorst, W., Webster, I., Weslawski, J.M., Wiberg, P., Sundby, B., 2001. Permeable marine sediments: Overturning an old paradigm. Eos, Trans. Am. Geophys. Union 82, 133–136. doi:10.1029/EO082I011P00133-01

Briggs, M., Lautz, L.K., Buckley, S.F., Lane, J.W., 2014. Practical limits on the use of diurnal temperature signals to quantify groundwater upwelling. Journal of Hydrology, 519B, 1739-1751.

Cable, J.E., Bugna, G.C., Burnett, W.C., Chanton, J.P., 1996. Application of 222Rn and CH4 for assessment of groundwater discharge to the coastal ocean. Limnol. Oceanogr. 41, 1347–1353.

Cable, J.E., Martin, J.B., 2008. In situ evaluation of nearshore marine and fresh pore water transport into Flamengo Bay, Brazil. Estuar. Coast. Shelf Sci. 76, 473–483. doi:10.1016/j.ecss.2007.07.045

Cable, J.E., Martin, J.B., Jaeger, J., 2006. Exonerating Bernoulli? On evaluating the physical and biological processes affecting marine seepage meter

664 measurements. Limnol. Oceanogr. Methods 4, 172–183.
665 doi:10.4319/lom.2006.4.172

666 Cai, P., Shi, X., Moore, W.S., Peng, S., Wang, G., Dai, M., 2014. 224Ra:228Th
667 disequilibrium in coastal sediments: Implications for solute transfer across
668 the sediment–water interface. Geochim. Cosmochim. Acta 125, 68–84.
669 doi:10.1016/j.gca.2013.09.029

670 Cai, P., Shi, X., Hong, Q., Li, Q., Liu,L., Guo, X., Dai, M., 2015. Using 224Ra/228Th
671 disequilibrium to quantify benthic fluxes of dissolved inorganic carbon and
672 nutrients into the Pearl River Estuary. Geochim. Cosmochim. Acta 170, 188-
673 203

674 Cai P., Shi, X., Moore, W.S., Dai, M., 2012. Measurement of 224Ra:228Th
675 disequilibrium in coastal sediments using a delayed coincidence counter.
676 Marine Chemistry, 138-139, 1-6.

677 Choi, J., Harvey, J.W., Conklin, M.H., 2000. Characterizing multiple timescales of
678 stream and storage zone interaction that affect solute fate and transport in
679 streams. Water Resour. Res. 36, 1511–1518. doi:10.1029/2000WR900051

680 Colbert, S.L., Hammond, D.E., 2008. Shoreline and seafloor fluxes of water and
681 short-lived Ra isotopes to surface water of San Pedro Bay, CA. Mar. Chem. 108,
682 1–17. doi:10.1016/j.marchem.2007.09.004

683 Colbert, S.L., Hammond, D.E., 2007. Temporal and spatial variability of radium in
684 the coastal ocean and its impact on computation of nearshore cross-shelf
685 mixing rates. Cont. Shelf Res. 27, 1477–1500. doi:10.1016/j.csr.2007.01.003

686 Cook, P.G., Lamontagne, S., Berhane, D., Clark, J.F., 2006. Quantifying groundwater
687 discharge to Cockburn River, southeastern Australia, using dissolved gas
688 tracers 222 Rn and SF 6. Water Resour. Res. 42, n/a–n/a.
689 doi:10.1029/2006WR004921

690 Fram, J.P., Pawlak, G.R., Sansone, F.J., Glazer, B.T., Hannides, A.K., 2014. Miniature
691 thermistor chain for determining surficial sediment porewater advection.
692 Limnol. Oceanogr. Methods 12, 155–165. doi:10.4319/lom.2014.12.155

693 Freeze, R.A., Cherry, J.A., 1979. Groundwater. Prentice-Hall, New Jersey.

694 Gelhar, L.W., Welty, C., Rehfeldt, K.R., 1992. A critical review of data on field-scale
695 dispersion in aquifers. Water Resour. Res. 28, 1955–1974.
696 doi:10.1029/92WR00607

697 Genereux, D.P., Hemond, H.F., Mulholland, P.J., 1993. Use of radon-222 and calcium
698 as tracers in a three-end-member mixing model for streamflow generation on
699 the West Fork of Walker Branch Watershed. J. Hydrol. 142, 167–211.
700 doi:10.1016/0022-1694(93)90010-7

701 Gonneea, M.E., Morris, P.J., Dulaiova, H., Charette, M.A., 2008. New perspectives on
702 radium behavior within a subterranean estuary. Mar. Chem. 109, 250–267.
703 doi:10.1016/j.marchem.2007.12.002

704 Gooseff, M.N., Wondzell, S.M., Haggerty, R., Anderson, J., 2003. Comparing transient
705 storage modeling and residence time distribution (RTD) analysis in
706 geomorphically varied reaches in the Lookout Creek basin, Oregon, USA. Adv.
707 Water Resour. 26, 925–937. doi:10.1016/S0309-1708(03)00105-2

708 Harrington, G.A., Walker, G.R., Love, A.J., Narayan, K.A., 1999. A compartmental
709 mixing-cell approach for the quantitative assessment of groundwater
710 dynamics in the Otway Basin, South Australia. J. Hydrol. 214, 49–63.
711 doi:10.1016/S0022-1694(98)00243-1

712 Huettel, M., Berg, P., Kostka, J.E., 2014. Benthic exchange and biogeochemical
713 cycling in permeable sediments. Ann. Rev. Mar. Sci. 6, 23–51.
714 doi:10.1146/annurev-marine-051413-012706

715 Huettel, M., Rusch, A., 2000. Transport and degradation of phytoplankton in
716 permeable sediment. Limnol. Oceanogr. 45, 534–549.

717 Huettel, M., Webster, I., 2001. Porewater flow in permeable sediments, in:
718 Boudreau, B.P., Jorgensen, B.B. (Eds.), The Benthic Boundary Layer. Oxford
719 Univ. Press, pp. 144–179.

720 Huettel, M., Ziebis, W., Forster, S., 1996. Flow-induced uptake of particulate matter
721 in permeable sediments. Limnol. Oceanogr. 41, 309–322.
722 doi:10.4319/lo.1996.41.2.0309

723

724 Huettel, M., Ziebis, W., Forster, S., Luther, G.W., 1998. Advective Transport Affecting
725 Metal and Nutrient Distributions and Interfacial Fluxes in Permeable
726 Sediments. Geochim. Cosmochim. Acta 62, 613–631. doi:10.1016/S0016-
727 7037(97)00371-2

728 Jahnke, R., Richards, M., Nelson, J., Robertson, C., Rao, A., Jahnke, D., 2005. Organic
729 matter remineralization and porewater exchange rates in permeable South
730 Atlantic Bight continental shelf sediments. Cont. Shelf Res. 25, 1433–1452.
731 doi:10.1016/j.csr.2005.04.002

732 Jahnke, R.A., Nelson, J.R., Marinelli, R.L., Eckman, J.E., 2000. Benthic flux of biogenic
733 elements on the Southeastern US continental shelf: influence of pore water
734 advective transport and benthic microalgae. Cont. Shelf Res. 20, 109–127.
735 doi:10.1016/S0278-4343(99)00063-1

736 Key, R.M., Guinasso, N.L., Schink, D.R., 1979. Emanation of radon-222 from marine
737 sediments. Marine Chemistry, 7, 221-250

738 Kirchner, G., 1998. Applicability of compartmental models for simulating the
739 transport of radionuclides in soil. J. Environ. Radioact. 38, 339–352.
740 doi:10.1016/S0265-931X(97)00035-0

741 Kirk, S.T., Campana, M.E., 1990. A deuterium-calibrated groundwater flow model of
742 a regional carbonate-alluvial system. J. Hydrol. 119, 357–388.
743 doi:10.1016/0022-1694(90)90051-X

744 Lamontagne, S., Cook, P.G., 2007. Estimation of hyporheic water residence time in
745 situ using ^{222}Rn disequilibrium. Limnol. Oceanogr. Methods 5, 407–416.
746 doi:10.4319/lom.2007.5.407

747 Li, Y.-H., Gregory, S., 1974. Diffusion of ions in sea water and in deep-sea
748 sediments. Geochim. Cosmochim. Acta 38, 703–714. doi:10.1016/0016-
749 7037(74)90145-8

750 Martin, J.B., Cable, J.E., Smith, C., Roy, M., Cherrier, J., 2007. Magnitudes of
751 submarine groundwater discharge from marine and terrestrial sources:
752 Indian River Lagoon, Florida. Water Resour. Res. 43, n/a–n/a.
753 doi:10.1029/2006WR005266

754 Neuman, S.P., 1990. Universal scaling of hydraulic conductivities and dispersivities
755 in geologic media. Water Resour. Res. 26, 1749–1758.
756 doi:10.1029/WR026i008p01749

757 Precht, E., Franke, U., Polerecky, L., Huettel, M., 2004. Oxygen dynamics in
758 permeable sediments with wave-driven pore water exchange. Limnol.
759 Oceanogr. 49, 693–705. doi:10.4319/lo.2004.49.3.0693

760 Precht, E., Huettel, M., 2004. Rapid wave-driven advective pore water exchange in
761 a permeable coastal sediment. J. Sea Res. 51, 93–107.
762 doi:10.1016/j.seares.2003.07.003

763 Precht, E., Huettel, M., 2003. Advective pore-water exchange driven by surface
764 gravity waves and its ecological implications. Limnol. Oceanogr. 48, 1674–
765 1684. doi:10.4319/lo.2003.48.4.1674

766 Qian, Q., Clark, J.J., Voller, V.R., Stefan, H.G., 2009. Depth-Dependent Dispersion
767 Coefficient for Modeling of Vertical Solute Exchange in a Lake Bed under
768 Surface Waves. J. Hydraul. Eng. 135, 187–197. doi:10.1061/(ASCE)0733-
769 9429(2009)135:3(187)

770 Qian, Q., Voller, V.R., Stefan, H.G., 2008. A vertical dispersion model for solute
771 exchange induced by underflow and periodic hyporheic flow in a stream
772 gravel bed. Water Resour. Res. 44, n/a–n/a. doi:10.1029/2007WR006366

773 Reimers, C.E., Stecher, H.A., Taghon, G.L., Fuller, C.M., Huettel, M., Rusch, A.,
774 Ryckelynck, N., Wild, C., 2004. In situ measurements of advective solute

transport in permeable shelf sands. Cont. Shelf Res. 24, 183–201. doi:10.1016/j.csr.2003.10.005

Riedl, R.J., Huang, N., Machan, R., 1972. The subtidal pump: a mechanism of interstitial water exchange by wave action. Mar. Biol. 13, 210–221. doi:10.1007/BF00391379

Rocha, C., 2008. Sandy sediments as active biogeochemical reactors: compound cycling in the fast lane. Aquat. Microb. Ecol. 53, 119–127. doi:10.3354/ame01221

Santos, I.R., Eyre, B.D., Huettel, M., 2012. The driving forces of porewater and groundwater flow in permeable coastal sediments: A review. Estuar. Coast. Shelf Sci. 98, 1–15. doi:10.1016/j.ecss.2011.10.024

Savidge, W., Gargett, A., Jahnke, R., Nelson, J., Savidge, D., Short, R., Voulgaris, G., 2008. Forcing and Dynamics of Seafloor-Water Column Exchange on a Broad Continental Shelf. Oceanography 21.

Savidge, W.B., Wilson, A., Woodward, G., 2016. Using a Thermal Proxy to Examine Sediment–Water Exchange in Mid-Continental Shelf Sandy Sediments. Aquat. Geochemistry 22, 419–441. doi:10.1007/s10498-016-9295-1

Shanahan, P., Harleman, D.R.F., 1984. Transport in Lake Water Quality Modeling. J. Environ. Eng. 110, 42–57. doi:10.1061/(ASCE)0733-9372(1984)110:1(42)

Stieglitz, T.C., van Beek, P., Souhaut, M., Cook, P.G., 2013. Karstic groundwater discharge and seawater recirculation through sediments in shallow coastal Mediterranean lagoons, determined from water, salt and radon budgets. Mar. Chem. 156, 73–84. doi:10.1016/j.marchem.2013.05.005

Webster, I.T., 2003. Wave Enhancement of Diffusivities within Surficial Sediments. Environ. Fluid Mech. 3, 269–288. doi:10.1023/A:1023694011361

Wilson, A.M., Woodward, G.L., Savidge, W.B., 2016. Using heat as a tracer to estimate the depth of rapid porewater advection below the sediment–water interface. J. Hydrol. 538, 743–753. doi:10.1016/j.jhydrol.2016.04.047

Xu, S., Wörman, A., Dverstorp, B., 2007. Criteria for resolution-scales and parameterisation of compartmental models of hydrological and ecological mass flows. J. Hydrol. 335, 364–373. doi:10.1016/j.jhydrol.2006.12.004

8. ACKNOWLEDGEMENTS

This research is a contribution to the ANR @RAction chair medLOC (ANR-14-ACHN-0007-01) and Labex OT-Med (ANR-11-LABEX-0061, part of the ‘‘Investissements d’Avenir” program through the A*MIDEX project ANR-11- IDEX-0001-02), funded by the French National Research Agency (ANR). PC acknowledges support from IméRA (Institute of Advacned Studies), Aix-Marseille Université (Labex RFIEA and ANR “Investissements d'avenir”). This project has received funding from the European Union’s Horizon 2020 research and innovation programme under the Marie Skłodowska-Curie grant agreement No 748896. We thank Jordi Garcia-Orellana and Joan Manuel Bruach from the Universitat Autònoma de Barcelona for radon sample analyses.

822 9. FIGURE LEGENDS

823

824 Figure 1. Schematic representation of advective mixing cell model. Arrows denote
825 flow directions during the first phase the recirculation cycle, in which flows are
826 downwards on the LHS and upward on the RHS. (The flow direction is reversed
827 during the second phase of the cycle.) Vertical water fluxes into and out of cell i are
828 $q_v(i\text{-}1)$ and $q_v(i)$, where i = 1,…n, where n+1 is the number of cells in the vertical
829 dimension. The horizontal flux between downwelling and upwelling profiles is
830 denoted $q_h(i)$. Concentrations in cell i are $c_a(i)$ and $c_b(i)$ on LHS and RHS
831 respectively. $c(0)$ is the concentration in surface water.

832

833 Figure 2. Observed radon profiles at two different locations within La Palme
834 Lagoon. The error bars represent the analytical uncertainties (1σ) for radon
835 (liquid scintillation counting).

836

837 Figure 3. (a) Mean vertical water velocity (upward or downward), as a function of
838 depth, and resulting radon concentration profile for $t_r/2 = 10^{-5}$ d (0.86 s) for Pz1.
839 The mean vertical water velocity is described by an exponential decrease in depth,
840 according to $\overline{q_v}(z) = \overline{q_v}(0)e^{-kz}$. The best-fit to the data is produced with k = 5 m^{-1}
841 and $\overline{q_v}(0)$= 0.25 m d^{-1}. Other parameters are γ = 900 Bq m^{-3} d^{-1} and θ = 0.4.

842

843 Figure 4. Sensitivity of radon profiles to recirculation times (t_r). Upwelling and
844 downwelling profiles following complete cycles of (a) t_r = 0.2 days (reversing every
845 0.1 d), (b) t_r = 2 days and (c) t_r = 40 days are represented. Note that the results
846 obtained from a recirculation time of 40 days would be equivalent to those

847 obtained for larger cycles. Note also that the inflection point in the downwelling
848 profile is similar to the estimated water flux ($q_v(0)$) multiplied by the period of
849 downwelling ($t_r/2$). Other model parameters are the same as in Figure 3.
850
851 Figure 5. Sensitivity of radon profiles in Pz1 to (a) surface water – sediment
852 exchange flux ($\overline{q_v}(0)$), (b) attenuation of water flux with depth (k), and (c) implicit
853 dispersivity (α).
854
855 Figure 6: Simulated $\overline{q_v}$ at different depths from 4 different radon profiles that
856 could be accommodated within the analytical uncertainties of radon
857 measurements of Pz1. Orange and grey dots represent lower and upper bounds
858 (1σ), respectively, of the radon measurements. Model parameters are q=0.35,
859 k=0.5, γ=950 (Black line), q=0.35, k = 2, γ=1000 (Blue), q=0.2, k=0.5, γ=820 (Red),
860 q=0.15, k=15, γ=820 (Green). All simulations use θ = 0.4.
861
862 Figure 7. a) Calculated enhanced dispersion coefficient as a function of depth for
863 Pz1 and b) comparison of the water fluxes ($\overline{q_v}$) at different depths derived from
864 the dispersion approach (circles) and the advective cycling model (solid line).
865
866

867 Table 1. Measured values of porewater salinity and radon concentration.

868 Uncertainty for radon concentration represents one standard deviation.

Pz1			Pz2		
Depth (m)	Salinity (g/kg)	^{222}Rn (Bq m^{-3})	Depth (m)	Salinity (g/kg)	^{222}Rn (Bq m^{-3})
0	30.6	25 ± 10	0	37.2	89 ± 28
0.05	32.9	933 ± 152	0.10	38.1	1238 ± 185
0.10	30.8	1753 ± 218	0.15	38.1	1807 ± 216
0.15	31.3	2895 ± 280	0.20	38.3	1953 ± 231
0.20	30.8	3477 ± 327	0.30	38.6	2228 ± 247
0.30	30.7	4258 ± 393	0.50	38.9	1925 ± 372
0.50	37.7	4985 ± 496	0.80	51.6	2665 ± 276
0.80	84.5	4022 ± 478	0.13	62.2	2600 ± 275

869

870

871

872

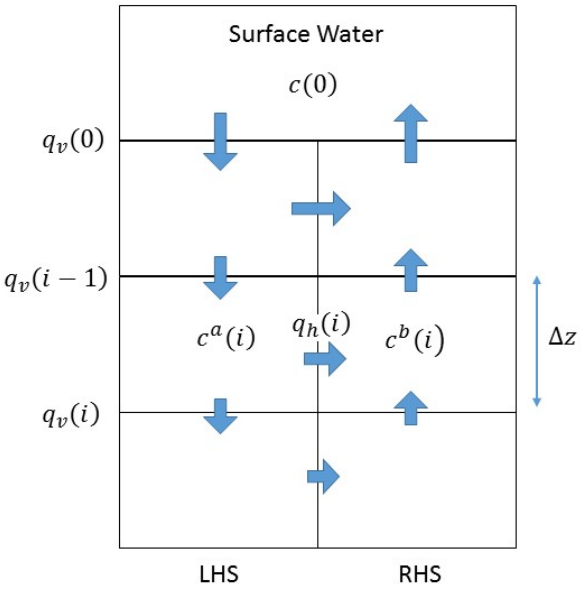

Figure 1. Schematic representation of advective mixing cell model. Arrows denote flow directions during the first phase the recirculation cycle, in which flows are downwards on the LHS and upward on the RHS. (The flow direction is reversed during the second phase of the cycle.) Vertical water fluxes into and out of cell i are $q_v(i\text{-}1)$ and $q_v(i)$, where i = 1,…n, where n+1 is the number of cells in the vertical dimension. The horizontal flux between downwelling and upwelling profiles is denoted $q_h(i)$. Concentrations in cell i are $c^a(i)$ and $c^b(i)$ on LHS and RHS respectively. $c(0)$ is the concentration in surface water.

888

889

890

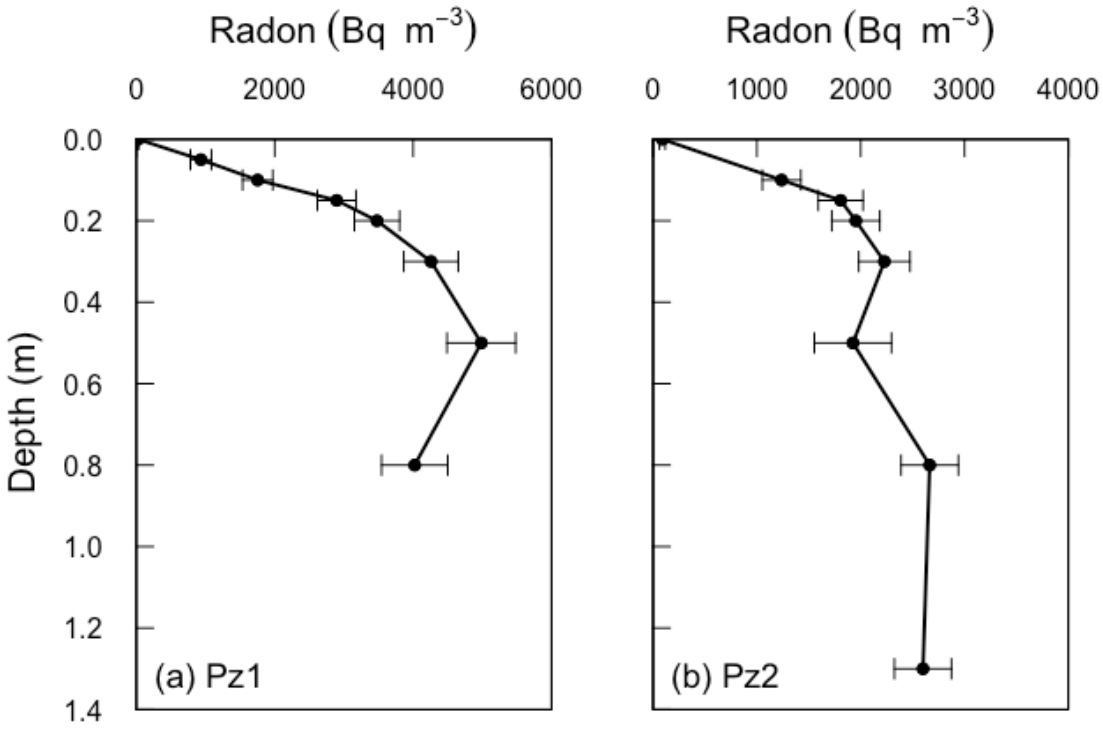

891

892

893 Figure 2. Observed radon profiles at two different locations within La Palme

894 Lagoon. The error bars represent the analytical uncertainties (1σ) for radon

895 (liquid scintillation counting).

896

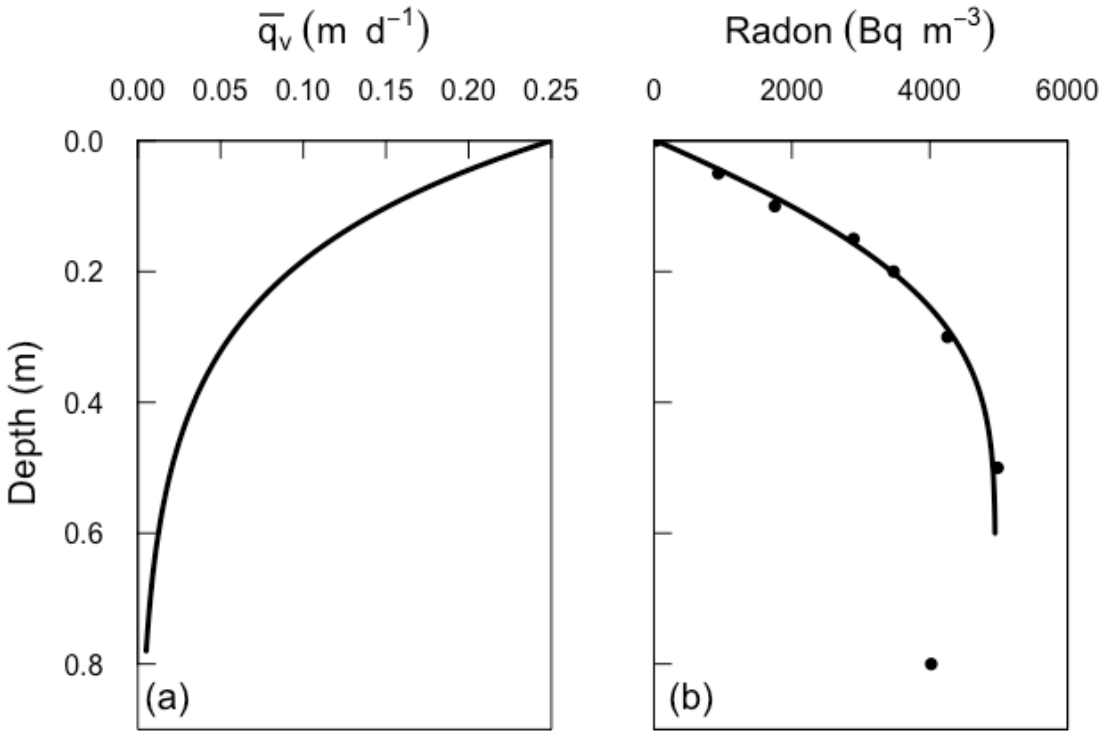

Figure 3. (a) Mean vertical water velocity (upward or downward), as a function of depth, and resulting radon concentration profile for $t_r/2$= 10^{-5} d (0.86 s) for Pz1. The mean vertical water velocity is described by an exponential decrease in depth, according to $\overline{q_v}(z) = \overline{q_v}(0)e^{-kz}$. The best-fit to the data is produced with k = 5 m^{-1} and $\overline{q_v}(0)$= 0.25 m d^{-1}. Other parameters are γ = 900 Bq m^{-3} d^{-1} and θ = 0.4.

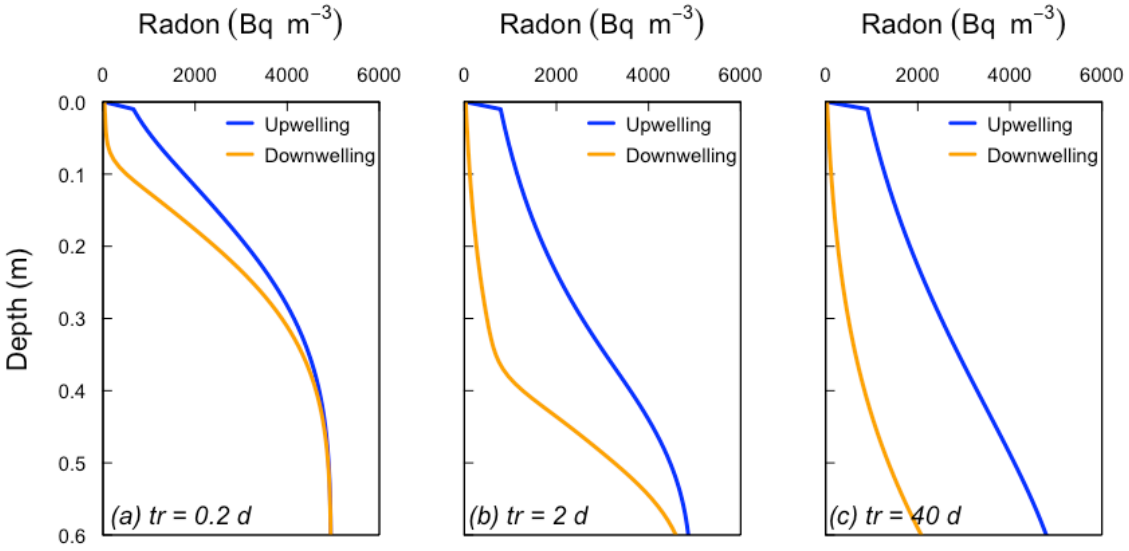

909

910

911

912 Figure 4. Sensitivity of radon profiles to recirculation times (t_r). Upwelling and
913 downwelling profiles following complete cycles of (a) t_r = 0.2 days (reversing every
914 0.1 d), (b) t_r = 2 days and (c) t_r = 40 days are represented. Note that the results
915 obtained from a recirculation time of 40 days would be equivalent to those
916 obtained for larger cycles. Note also that the inflection point in the downwelling
917 profile is similar to the estimated water flux ($q_v(0)$) multiplied by the period of
918 downwelling ($t_r/2$). Other model parameters are the same as in Figure 3.

919

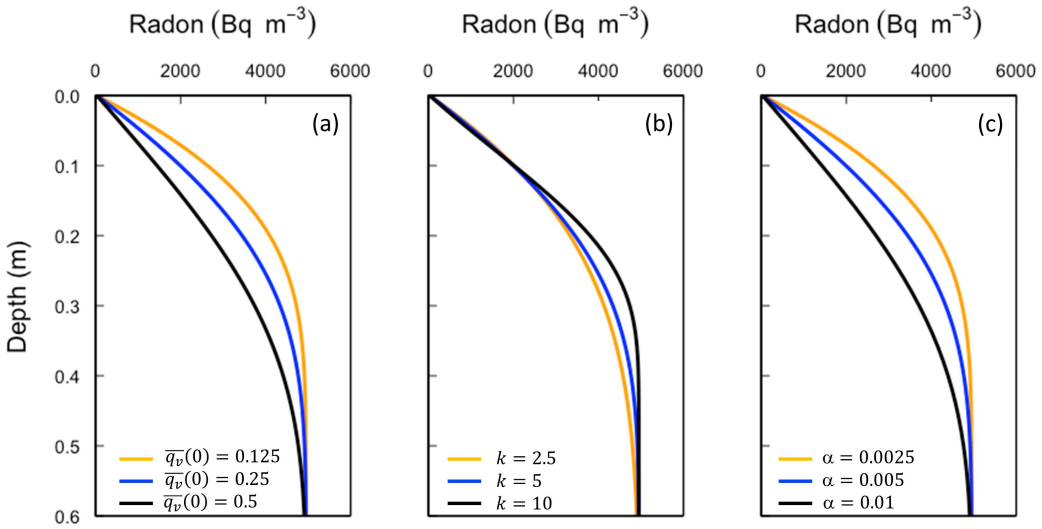

Figure 5. Sensitivity of radon profiles in Pz1 to (a) surface water – sediment exchange flux ($\overline{q_v}(0)$), (b) attenuation of water flux with depth (k), and (c) implicit dispersivity (α).

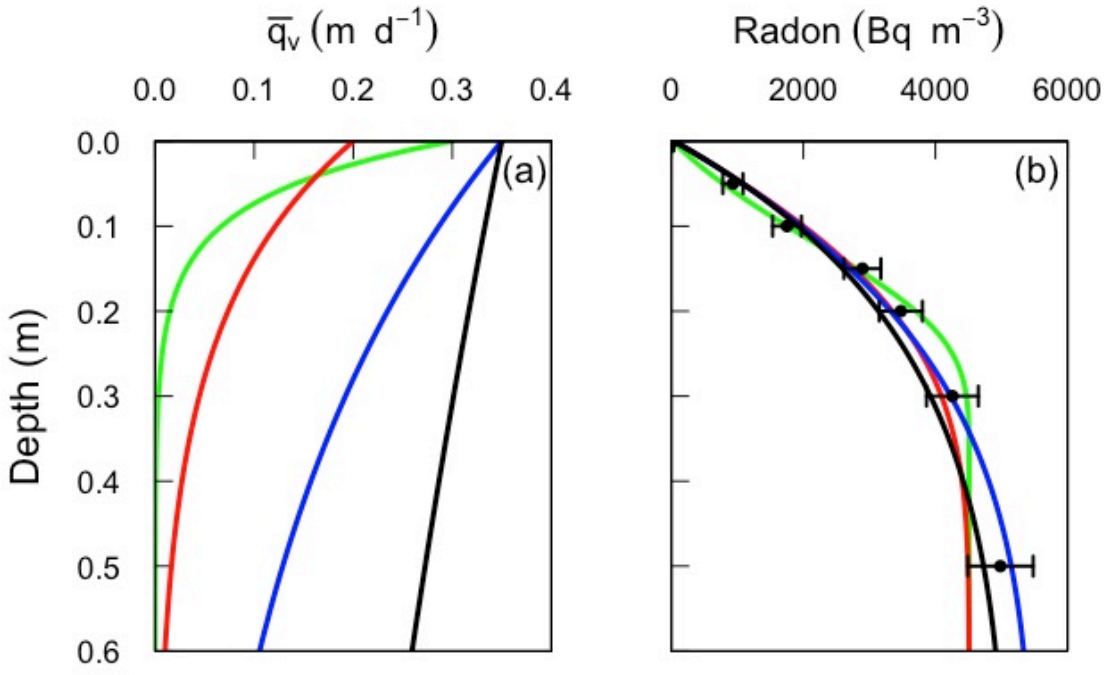

Figure 6: Simulated $\overline{q_v}$ at different depths from 4 different radon profiles that could be accommodated within the analytical uncertainties of radon measurements of Pz1. Model parameters are q=0.35, k=0.5, γ=950 (Black line), q=0.35, k = 2, γ=1000 (Blue), q=0.2, k=0.5, γ=820 (Red), q=0.15, k=15, γ=820 (Green). All simulations use θ = 0.4.

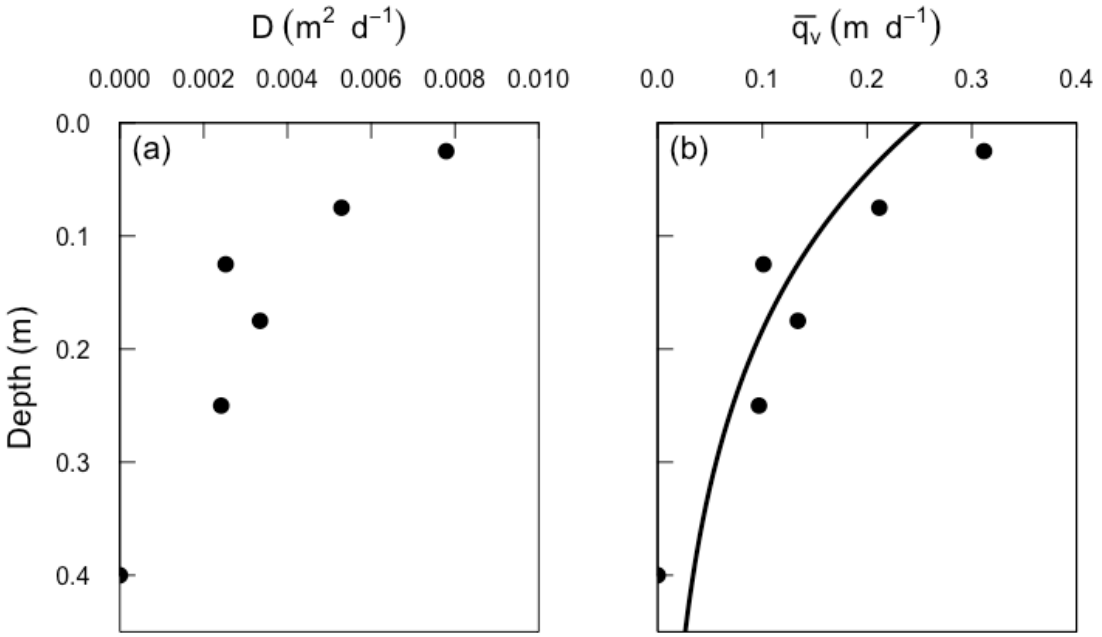

941

942

943

944

945

946 Figure 7. a) Calculated enhanced dispersion coefficient as a function of depth for

947 Pz1 and b) comparison of the water fluxes ($\overline{q_v}$) at different depths derived from

948 the dispersion approach (circles) and the advective cycling model (solid line).

949